Paper to be presented at the 2nd International Conference on Integrated Micro/Nanotechnology for Space Applications, MNT 99, April 11-15, 1999, Pasadena, CA

MEMS ~~ADVANCED~~ MICROPROPULSION ACTIVITIES AT JPL

Juergen Mueller, Indrani Chakraborty, Stephen Vargo, David Bame, Colleen Marrese, and William C. Tang

Jet Propulsion Laboratory
California Institute of Technology
Pasadena, CA 91109

A status of MEMS-based micropropulsion activities conducted at JPL will be given. These activities include work conducted on the so called Vaporizing Liquid Micro-Thruster (VLM) which recently underwent proof-of-concept testing, demonstrating the ability to vaporize water propellant at 2 W and 2 V. Micro-ion engine technologies, such as field emitter arrays and micro-grids are being studied. Focus in the field emitter area is on arrays able to survive in thruster plumes and micro-ion engine plasmas to serve as neutralizers and engine cathodes. Integrated, batch-fabricated ion repeller grid structures are being studied as well as different emitter tip materials are being investigated to meet these goals. A micro-isolation valve is being studied to isolate microspacecraft feed systems during long interplanetary cruises, avoiding leakage and prolonging lifetime and reliability of such systems. This concept relies on the melting of a thin silicon barrier. Burst pressure values as high as 2,900 psig were obtained for these valves and power requirements to melt barriers ranging between 10 - 50 μm in thickness, as determined through thermal finite element calculations, varied between 10 - 30 W to be applied over a duration of merely 0.5 ms

I.INTRODUCTION

Recently, a strong interest in micropropulsion devices has arisen within the space community, capable of delivering very small thrust values in the milli-Netwon range and below, and impulse bits on the order of micro-Newton-seconds at engine sizes and masses orders of magnitude smaller than available with current technologies[1]. Within the National Aeronautics and Space Administration (NASA) as well as the Air Force, the reason for this interest can be found both in the drive to explore microspacecraft designs[2], typically viewed as spacecraft having wet masses on the order of a few tens of kilograms and below, as well as in the need for ultra-fine attitude control of larger spacecraft, such as those envisioned for future NASA space interferometry missions[3], for example. The use of microspacecraft will reduce mission cost by reducing launch cost, but will also allow wholly new and unique mission profiles to be flown, involving constellations of microspacecraft charting entire regions of space, or increasing mission reliability by off-loading instruments from a large single spacecraft onto a fleet of microspacecraft. Thus, loss of a single microspacecraft will not endanger the entire mission. In military applications, constellations of microspacecraft are being envisioned to deploy phased antenna arrays for high-resolution radar observation of objects of military interest on Earth. Interferometry missions, on the other hand, will be used in the search for planets, and possibly even the evidence of life, around other stars, and are anticipated to play a central role in future NASA activities.

However, microspacecraft require radically new approaches in design, both on the system as well as component level. While significant progress in that direction is being made in the instrument, attitude sensing, as well as data handling and storage areas, for example, propulsion still appears to be lagging in this regard, offering only limited hardware choices able to fit the design constraints imposed by microspacecraft with respect to mass, size as well as power[1]. Virtually all propulsion subsystem areas, such as attitude control, primary propulsion and feed system components, are still in need for suitable design solutions.

One of the most challenging aspects of both mission types, microspacecraft and interferometry, is attitude control. Either due to the low mass of the microspacecraft, or the stringent pointing and positioning requirements of spacecraft used in constellations, very small impulse bits will be required, which could reach into the micro-Newton-second range. Furthermore, since multiple thrusters will be required for attitude control, thruster units will also have to be extremely small and light-weight to meet microspacecraft mass and volume design constraints. Similarly, power constraints will need to be adhered to. Total microspacecraft power levels may not exceed a few tens of Watts, possibly considerably less. While there is available today propulsion hardware able to deliver very small impulse bits, namely Pulsed Plasma Thrusters (PPT) or Field Emission Electric Propulsion (FEEP) devices[1], these thruster types may not fit every mission need. For microspacecraft applications, for example, micro-thrusters will not only be required for fine-pointing, but may also be needed to perform slew maneuvers. Depending on slew rates, required thrust levels for these maneuvers may reach well into the milli-Newton range, achievable with FEEP and PPT thrusters only at relatively high power levels and with large engine sizes. There also exists the need for thrusters using non-contaminating propellants, in particular in constellation flying applications where thrusters firing on one spacecraft may be pointed directly toward another spacecraft flying nearby in the constellation, possibly leading to contamination concerns. It is uncertain at this point whether FEEP or PPT thrusters may meet this requirement.

Cold gas systems exist that could deliver required thrust levels for slew maneuvers as well as small impulse bits on the order of 10^{-4} Ns[1]. In addition, cold gas propellants are considered non-contaminating for most mission applications. However, cold gas systems are plagued by propellant leakage concerns to a much higher degree than liquid systems are, possibly reducing the reliability and lifetime of the mission. In addition, high-pressure gaseous propellant storage will lead to large and heavy propellant tanks which may completely dominate microspacecraft layout and possibly require substantial compromises with respect to other subsystems in its design.

Within the primary propulsion area high specific impulse options appear to be of particular interest, since their ability to conserve considerable amounts of propellant mass may have a significant bearing on microspacecraft design. Currently among the most mature high-specific-impulse (Isp) propulsion technologies is ion propulsion, as evidenced by the recent flight of this technology on NASA's Deep Space 1 (DS-1) mission. Presently available engine technology, however, is relatively large, extending from beam diameters of 30 cm in case of the DS-1 engine, down to about 10-cm, and requiring power levels on the order of several thousands to several hundreds of Watts[1]. Thus, there obviously exists a need to further miniaturize this technology to make it more amenable to the aforementioned mission categories. Other competing thruster options, such as the aforementioned Field Emission Electric Propulsion (FEEP) and Pulsed Plasma Thruster (PPT) may provide relatively high specific impulses and could potentially be used as microspacecraft primary propulsion devices despite their low thrust levels due to the low expected spacecraft masses. However, micro-ion engine technology, if it can be successfully developed, will be characterized by a unique combination of high specific impulse capability, the use of inert, non-contaminating propellants, higher thrust-to-power ratios than obtainable with FEEP or PPT systems, and, unlike in the case of the inherently pulsed PPT devices, a continuous mode of operation.

At JPL, as well as other institutions around the country and abroad, searches for more suitable micropropulsion technologies is underway. Increasingly, these technologies include microfabrication or Microelectromechanical Systems (MEMS) approaches in order to achieve the

high degrees of miniaturization required. Although MEMS is not a prerequisite for micropropulsion concepts - indeed there exist concepts today, such as various miniature cold gas thrusters, among others, which appear to meet microspacecraft design constraints without resorting to such technologies[1] - MEMS does offer several unique advantages. In oder to distinguish these MEMS-based approaches, which will require substantial advances in fabrication, integration, as well as diagnostics, from more conventiaonl approaches, these activities have been termed "advanced micropropulsion" in this paper. In the following, some of these advantages, as well as challenges facing MEMS propulsion, are reviewed and several MEMS propulsion concepts currently being studied at JPL are described.

II. OVERVIEW OF MEMS PROPULSION ACTIVITIES

The Case for MEMS-Propulsion

The use of MEMS technology does offer the obvious benefit of creating extremely small and light weight devices. For microspacecraft in the 1- kg mass range such technologies may be a prerequisite to meet the stringent mass and volume constraints, in particular for attitude control applications were multiple thruster units will be required. However, it has been pointed out within the micropropulsion community - and justifiable so - that while MEMS-based components may achieve very high degrees of miniaturization, the finally assembled device, featuring necessary protective covers, electrical interfaces and propellant feeds, may not be significantly smaller and lighter than more conventionally machined, miniature thruster components available today. For example, cold gas thrusters featuring miniature solenoid valves weighing as little as 7 g have been successfully fabricated using non-MEMS fabrication techniques[4]. Using MEMS-based propulsion components, however, will allow for an extremely high degree of integration among different propulsion system components as well as control electronics, and thus offer significant additional mass and volume savings even over miniature non-MEMS components. For example, a MEMS-based thruster may be directly bonded to a MEMS-based valve or filter chip. Control electronics may be integrated onto the individual component chips, and the whole unit may then be packaged into an extremely compact module with minimal external interfaces, easing, and reducing the cost of, integration into the microspacecraft. The latter point will be of increasing importance for extremely small microspacecraft designs, such as those in the sub-10 kg mass range. Here, it may no longer be feasible or practical to rout miniature feed lines throughout the microspacecraft and to individually weld and plum components together.

Finally, for certain applications, MEMS-based components may offer performance advantages, such as in the case of attitude control thrusters. The need to provide extremely small impulse bits may be addressed by micro-fabricating very small nozzle throats through which a propellant may be thermally expanded. If paired with fast acting valve technology, achievable impulse bits may be reduced significantly over values obtainable with current chemical or cold gas technology. On the other hand, nozzle-based chemical or electrothermal thruster concepts will exhibit higher thrust-to-power ratios than electrostatic or electromagnetic thruster concepts, such as FEEPs, colloid thrusters, or PPTs, for example, and may thus be able to produce the thrust levels required for microspacecraft slew maneuvers as well.

MEMS-based propulsion concepts, however, will also face many design challenges. Since silicon is the primary building material of choice in MEMS technology today, based on considerable experience acquired with this material over the past couple of decades in the MEMS field, material compatibility issues between silicon, or certain thin films deposited onto silicon, such as silicon oxide or silicon nitride, and various propellants will need to be explored. Silicon also is a very good thermal conductor (with a thermal conductivity of about 150 W/mK) and its use may thus lead to thermal design challenges since thruster applications generate heat that needs to be contained within the device as much as possible to maintain high thruster efficiencies. Further, although silicon has very high yield strengths, approaching those of stainless steel, silicon is brittle, and internal pressurization, such as required in propulsion applications, will need to be carefully examined. Recent tests performed under static (non-vibrating) test conditions, however,

have yielded very high burst pressures of almost 3,000 psig for an internally pressurized isolation valve concept[5]. Finally, integration between silicon and non-silicon (mostly metal) components will need to be addressed since propellant tanks, due to the required size, will likely be fabricated using more conventional techniques for the foreseeable future. Non-silicon based microfabrication methods may also need to be explored to avoid some of the design challenges discussed for conditions were silicon-based fabrication is unacceptable. This in turn will likely require a substantial amount of additional basic fabrication process development.

The Brief History of MEMS-Propulsion

The first MEMS-based propulsion was apparently proposed by Mitterauer in 1991[6] in the form of a microfabricated FEEP thruster concept study based on field emitter array technology. The purpose of the design study was to further decrease mass and size of this concept and take advantage of the fact that critical thruster dimensions, such as the emitter slit height, were already in the micrometer range even for conventional designs. Shortly thereafter, in 1994, at the Aerospace Corporation, Janson[7] extended the vision for MEMS-based propulsion concepts to other devices as well, such as MEMS-based resistojets and ion propulsion. These activities were part of a more comprehensive study to investigate microspacecraft designs entirely based on MEMS fabrication techniques[7]. Microspacecraft concepts had also been studied at the Jet Propulsion Laboratory (JPL) at this point, primarily by Jones[8-14] as well as others[15,16]. As part of this ongoing activity, a study was conducted at JPL in 1995 to investigate the feasibility of microspacecraft concepts with masses between 15 kg and < 1 kg[17,18]. Several MEMS-based propulsion concepts were conceived and proposed in this study, including MEMS-based phase-change thruster concepts using liquid[19] and solid propellants, as well as microvalves[5]. At about the same time, MEMS-based cold gas thruster concepts were conceived and pursued in Europe, in a collaboration between the European Space Agency (ESA) and ACR Electronic Company in Sweden[20-22], and a MEMS-based solid rocket motor array concept had been initiated in France under funding by the Centre National d'Etudes Spatiales (CNES)[23].

These early activities were soon followed by a flurry of different micropropulsion projects at various private companies, university laboratories and governmental institutions. Private companies pursuing MEMS propulsion include, in the US, TRW[24] and Honeywell[25] pursuing so called "digital array" thruster concepts consisting of an array of a multitude of microfabricated, single-shot thrusters, Marotta Scientific Controls developing a MEMS-hybrid cold gas thruster featuring a microfabricated nozzle inlet, Phrasor Scientific[26] studying MEMS-fabricated colloid thruster concepts, SRI[27] studying micro-FEEP concepts, and, in Italy, Centrospazio[28] investigating micro-FEEP thrusters as well. Among university laboratories work is currently performed at MIT[29-32], studying micro-nozzle flows as well as micro-bipropellant engines (work is also performed at MIT on a miniature Hall thruster, however, this concept is not MEMS-based[33-35]), the University of Southern California (USC)[36] investigating micro-ion engine concepts and micro-resistojets, and Princeton University[25] working in collaboration with Honeywell on digital thruster arrays, as well as performing high-resolution thrust stand measurements. Government institutions performing MEMS-related propulsion work include the Air Force Research Laboratory (AFRL)[37,38] pursuing projects on micro-resistojets and micro-ion engines, in part in collaboration with USC, as well as (non-MEMS based) on Pulsed Plasma Thrusters (PPT), and NASA Lewis Research Center[32,39], studying digital thruster array concepts as well. In addition continued work is performed by the aforementioned players, i.e. the Aerospace Corporation[7,40-42], ESA[20-22], CNRS[23], and JPL[5,19,43-45]. In the following, the work at JPL will be discussed in greater detail and recent accomplishments will be presented.

III. THE VAPORIZING LIQUID MICRO-THRUSTER

The Vaporizing Liquid Micro-Thruster (VLM) is aimed at providing attitude control for microspacecraft. This microfabricated thruster concept is targeted to provide very small thrust values in the range of 0.1 - 1 mN and impulse bits in the 10^{-7} - 10^{-5} Ns range (depending on the

valve used) at extremely low thruster weight and size, able to be placed onto a silicon chip. In this thruster concept propellant will be vaporized on demand, generating thrust by thermally expanding propellant vapor through a nozzle. The propellant can be stored compactly in its liquid phase using light-weight, low-pressure tanks and leakage concerns can be significantly reduced or eliminated due to liquid storage. Development of the VLM is in its earliest stages. Initial focus of VLM-related work is the determination of the feasibility of this thruster concept, to be followed up by the determination of its performance and operating characteristics in the future.

The Vaporizing Liquid Micro-Thruster concept, in its current configuration, relies in its construction on silicon-based microfabrication (MEMS - Microelectromechanical Systems) methods and is shown in Fig. 1. A completed chip is shown in Fig. 2. The VLM operates by vaporizing a suitable liquid propellant inside a micro-machined, thin-film deposited heater. Water, ammonia, and hydrazine are currently under consideration as propellants, although in principle any propellant that can be vaporized, and does not exhibit compatibility issues with the materials of construction, may be used. As a result of the microfabrication techniques employed in its fabrication, extremely small thruster size and weights can be achieved. Chip weight is a few grams, and current chip sizes are about 0.9 x 1.5 x 0.1 cm^3, with a slightly smaller version of 1 x 1.1 x 0.1 cm^3 currently under construction. Thrust and impulse bit values have not been measured yet at this stage of the development. However, targeted performance data for the VLM are thrust values of 0.1 to 1 mN and impulse bit values of 10^{-7} to 10^{-5} Ns (depending on available valve technology). Input power levels and voltage bus requirements have to be minimized to take into account limited onboard power levels and the trend towards lower bus voltages on microspacecraft. Vaporization of propellant (water) has been achieved at power levels around 2 W and voltages of slightly under 2 V. During these tests, the thruster chips were mounted onto a test rig consisting of a water tank, a 2-micron filter placed at the tank outlet, and a small commercial solenoid valve manufactured by the Lee Company. The packaged chip assembly was mounted onto a port via a threaded aluminum or Vespel nut bonded to the chip carrier (see Fig. 3). A pressurant supply was connected to the water tank. By pressurizing the tank, water is forced through the filter and valve and into the chip.

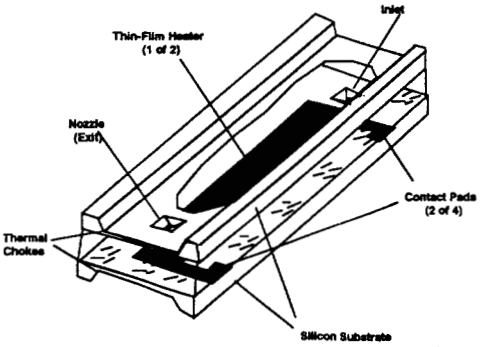

Fig. 1: Concept of the Vaporizing Liquid Micro-Thruster

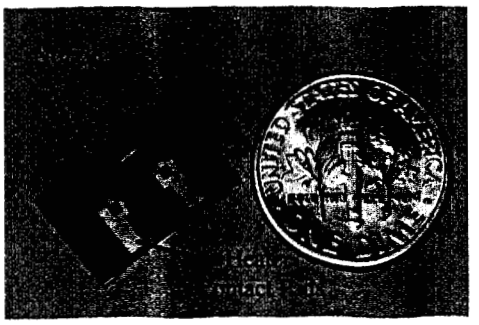

Fig. 2: Vaporizing Liquid Micro-Thruster Chip

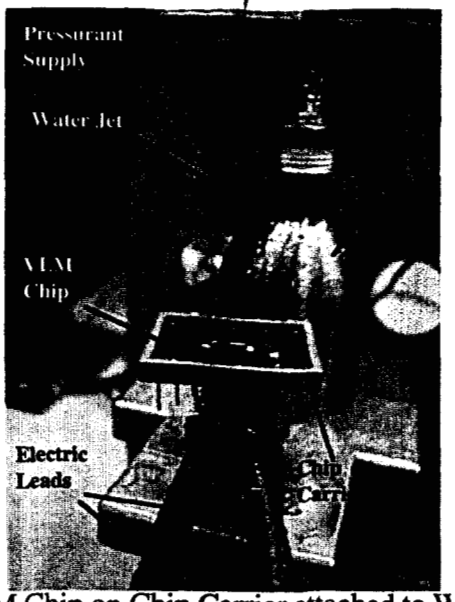

Fig. 3: VLM Chip on Chip Carrier attached to Water Tank.
Notice Water Jet Exciting Nozzle a Result of No Heat Input to Chip.

Obviously, the concept of heating a working fluid in a heat exchanger element and expelling it to produce thrust is not new and has been exploited in resistojet designs for many years, although many of these designs have employed gaseous propellants[46]. The uniqueness, and challenge, of the VLM lies in adapting this concept, using liquid propellants for compact propellant storage and reduced leakage rates, and employing it to microscale devices featuring heater lengths no more than a few millimeter in length. Until the successful conduction of experiments to be discussed in this paper it was not certain whether vaporization of propellant could be achieved over such short distances.

Proof-of-concept demonstration was recently attained with a series of VLM chips, demonstrating the complete vaporization of water inside the thruster chip. The thruster chips used are shown in Table 1. Chip design variations included different channel layouts (mostly straight channels, one chip featured a meandering channel design), different channel lengths and heights, as well as different packaging. In these tests, differences in packaging were limited to the use of different interconnecting nuts (either aluminum or Vespel) with which the chip could be interfaced with its feed system.

Table 1: VLM Chip Test Articles

Designation	Heater Length (mm)	Channel Cross Section (μm^2)	Channel Type	Fixture Material
SC-4-600-Al	4	950 x 600	Straight	Aluminum
SC-4-600-V	4	950 x 600	Straight	Vespel
SC-5-300-V	5	950 x 300	Straight	Vespel
SC-5-300-V/Poly*	5 (PolySi)	950 x 300	Straight	Vespel
SC-6-300-V	6	950 x 300	Straight	Vespel
MC-12--300-V	12.16	400 x 300	Meandering	Vespel

*featuring a heater made from polysilicon. All other heaters made from gold.

Preliminary test data obtained with these chips are shown in Figs. 4 and 5. The first tests, conducted using chips featuring a 600 μm channel height and packaged using the aluminum nut resulted in relatively high required power levels at extremely low feed pressures to achieve vaporization. The VLM required 7 W at about 0.25 psig feed pressure[19]. This data point is shown in the upper left hand corner of Fig 4. As mentioned, this chip featured an aluminum nut, which had been identified as a major heat sink due to the poor insulation provided by the ceramic carrier package. Replacing the aluminum nut with one machined out of Vespel material reduced required power levels dramatically by about 30% to just under 5 W at the same feed pressure. Using this chip assembly, vaporization was still possible at a feed pressure more than twice that value (0.64 psig) at about 6.5 W. These power levels, however, were still approaching or exceeding the maximum targeted value (5W), and, under vaporization conditions, only very low feed pressures could be maintained resulting into only extremely low flow rates (although the latter could not be measured, when turning off the heater to observe purely liquid rates, only a small droplet could be seen forming at the nozzle outlet). In addition, vaporization was noted to be poor, and certainly not complete, as evidenced by a continuous sputtering noise and frequent visible liquid droplet ejections in addition to the steam generated.

The low required feed pressures were not expected. As a major concern in the development of the VLM had been anticipated high viscous losses, in particular in the case of liquid propellant flow. Consequently large channel cross had been conservatively chosen to accommodate the flow without encountering excessive flow resistances. This concern could clearly be dismissed after the

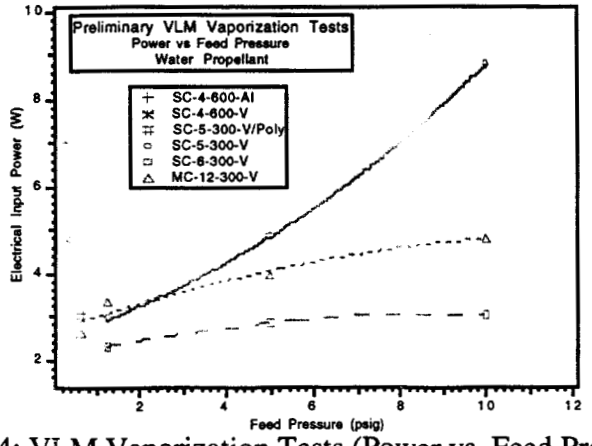

Fig. 4: VLM Vaporization Tests (Power vs. Feed Pressure)

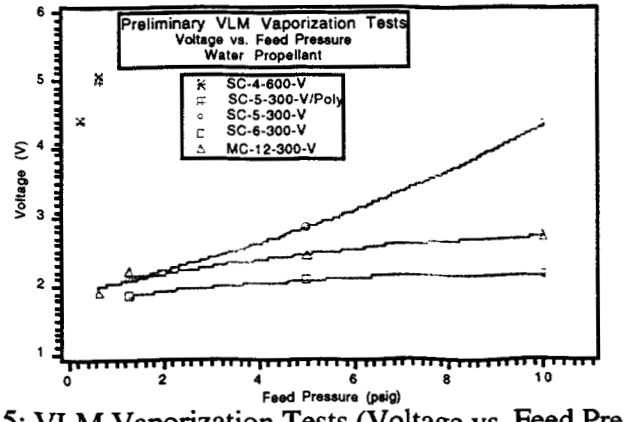

Fig. 5: VLM Vaporization Tests (Voltage vs. Feed Pressure)

described first set of tests. Thus, new VLM designs were fabricated and tested. These new chips featured shallower channel profiles with a height of 300 μm. The goal was to bring more liquid into more immediate contact with the heaters and thus effect a more efficient heat transfer.

Using the new chips, a significant improvement in performance could be noted. In contrast to tests conducted with chips featuring 600 μm channel heights, vaporization was, once a critical power level had been attained for a given feed pressure, complete. Exhaust was invisible and could only be evidenced by a cool glass slide placed into the vapor jet. No sputtering noises were heard. The critical power levels required to attain these conditions were also significantly lower than in earlier tests. For a chip featuring a 6 mm long heater, required power levels were only 2.3 W at about 1.3 psig feed pressure, increasing to 2.8 W at 5 psig feed pressure and 3 W at 10 psig feed pressure. These feed pressure values are within the realm of practical applicability, even for use in space systems, and power levels are well below the initially targeted value. In addition, voltage requirements in this case range just below or above 2 V, as can be seen in Fig. 5, depending on feed pressure, and are thus well within the capability of future microspacecraft.

Other chips featuring the same shallow channel profile (300 μm) resulted in somewhat higher power and voltage levels. In the case of a 5 mm heater, power levels were found to be somewhat higher, but are still well within the design targets, with the exception of one data point at a 10 psig feed pressure, in which case power requirements exceeded 8 W. This rather dramatic increase in power requirement with increased feed pressure (thus flow rate) for chips with shorter heater elements is reasonable, since less heat transfer to the liquid can occur over shorter heater lengths, requiring higher heater temperatures and power levels to achieve complete vaporization. However, even for this chip no more than 5 V were required.

In the case of the meandering channel design, superimposed on a 5 mm long heater element, required power levels were higher than in the 6-mm long heater design even though the flow path in the meandering channel design is less than half as wide and twice as long as in the 6-mm long straight channel design. This appears surprising and inconsistent, however, as noted above, due to the lack of suitable flow rate measurements a direct quantitative comparison between the different chip designs was not yet possible. Despite this lack of accurate flow measurements it was noted that the meandering channel design flowed considerable more liquid than the straight channel sections. While all other chips, even at the highest feed pressures, only formed a liquid droplet at the nozzle outlet in the unheated state, the meandering chip design emitted a water jet at the same pressures, similar to the one shown in Fig. 3. While this in itself is surprising, since higher flow resistance should have been expected in the meandering chip design, it does explain - at least qualitatively - the observed difference in required heater powers.

As a possible explanation for these observed differences in flow behavior for the different chips may be offered the potential of contamination located inside the narrow flow channels, either accumulated during handling and testing of the chip, or through the solidification of capillary-fed epoxy flow into the channel sections during bonding procedures. Poor alignment between the various vias in the different chip laminates and the ports machined into the carriers and connecting nuts may also have lead to local flow restrictions. In all cases, actual flow rates may be reduced due to locally decreased flow cross sections. So far, evidence of contamination during handling and testing may have been found in the case of one chip which seized conducting liquid during testing. The same chip featured a misalignment between the port machined into the chip carrier and the chip inlet hole, with the chip carrier surface partly covering the latter. In addition, one chip did not flow liquid at all, and contamination, if any, may have occurred prior to testing, possibly at some stage in the packaging phase, were chips leave the clean room environment. Once packaging is complete, chips are sealed in containers and not exposed to the environment prior to testing. Neither one of the failed chips is listed in Table 1 or Figs. 4 and 5, respectively.

Finally, a chip using a polysilicon heater was tested. This chip again featured a straight channel and a 5 mm long heater. When comparing power requirements of this chip with a chip featuring a 5-mm gold heater, they can be found to be very similar for nearly identical feed

pressures, as would be expected. However, when examining Fig. 5, it can be seen that the polysilicon chip has voltage requirements well exceeding those of the gold heater by more than a factor of two, i.e. about 5 V vs. 2 V in the case of the gold heater, at approximately the same power levels. These differences in voltage requirements are expected due to the higher resistance of polysilicon when compared with gold and are considered critical in view of microspacecraft applications.

Given the constraints placed on this first set of proof-of-concept experiments, the need for future work to improve the existing, very preliminary data base is obvious. Data obtained to date is very preliminary and in many cases does not yet allow for a quantitative comparison between different chip designs. To this end, first, methods have to be devised to measure extremely low liquid flow rates. The case of measuring liquid rates is made difficult by the fact that, unlike in the measurement of gaseous flow rates, much smaller volume displacements are encountered for a given mass flow rate. Other areas of future work include testing under vacuum conditions, thrust stand measurements, and continued optimization of chip designs as a result of the obtained measurements. An improved understanding of microchannel two-phase flow phenomena is highly desirable also. Currently, the state of knowledge in this area is poor. Existing literature in this area addresses some special cases, however, in many cases two-phase flow phenomena are not considered at all. An improved understanding of micro-channel two-phase flow physics is essential in designing improved VLM heater designs, offering the potential of lower power requirements or shortened vaporization channels, further decreasing chip sizes. Different propellants will need to be tested, in particular propellants having lower heat of vaporization than water, such as ammonia, which would result in additional power reductions for achieving vaporization. At this stage, detailed propellant compatibility studies will be required, and, if needed, appropriate chip coating techniques need to be explored to avoid chip erosion. Other issues to be addressed will be concerns related to the dribble volume, formed by the heater channel volume downstream of the thruster valve, which may broaden the thruster impulse bit. Although longer channels may be beneficial for vaporization reasons, they will increase the dribble volume unless channel cross sections are constrained. Deceased flow cross sections may lead to higher feed pressure requirements, which in view of the low feed pressures encountered so far could probably be accommodated. Last but not least, assuming that satisfactory performance of the VLM can be demonstrated, thruster integration with other feed system components as well as respective control electronics, on the same chip or through chip-to-chip bonding, will need to be addressed aggressively in order to reap one of the major benefits of a MEMS-based thruster over more conventional designs.

IV. MICRO-ION ENGINE TECHNOLOGIES

At the Jet Propulsion Laboratory there is currently underway a feasibility study to investigate the potential of reducing ion engine sizes dramatically below current state-of-the-art levels. Engine diameters in the 1-3 cm range and thrust levels in the sub-mN to few mN range are being targeted. In order to arrive at a functional ion engine of this small a size, however, several feasibility issues will need to be investigated and overcome. Among these are the sustainability and efficient operation of high surface-to-volume ratio plasma discharges, the replacement of hollow-cathode technologies with lower-power consuming and easier to miniaturize cathode systems to function both as engine cathodes and neutralizers, such as field emitter array technology, miniature accelerator grid system fabrication and operation, as well as the fabrication of miniaturized power conditioning units and feed system components. In this paper, the feasibility of microfabricated grid designs will be investigated from the perspective of obtainable grid breakdown voltages.

Field Emitter Arrays

A major part of this work will be the development of field emission arrays for application as low power, long life cathodes for the micro-ion engine. This part of the activity will seek to model, design, fabricate and test field emitter array cathode (FEAC) with a Cathode Lens and Ion

Repeller (CLAIR) electrode configuration which will focus the electron beams, provide independent control over the electron energy and shield the emitter surfaces from ion bombardment. The goal of this activity is to demonstrate a technology that will allow field emitter arrays to be used in environments where pressures are much greater than 10^{-5} Torr, which will in turn enable the development of micro-ion thrusters and more efficient cathodes for conventional electric thrusters

Field emitter cathode arrays are micron-sized, batch-fabricated structures with sharp conical electron emitting electrodes and gate electrodes with small apertures that extract electrons. A single element of an array is shown in Fig. 6. An array of these structures is shown in Fig. 7. Typical FEACs employ molybdenum or silicon tips fabricated by etching and deposition techniques. The emitter tips are typically ~1 mm tall, have a radius of curvature down to tens of angstroms, and can be fabricated in arrays with packing densities greater than 10^7 tips/cm^2. When the voltage bias on the gate electrode relative to the conical tip is sufficiently high, the electric field at the tip becomes high enough to extract electrons by field emission. In a properly designed array, gate voltages around 100 V are required to extract electron beams on the order of 1 microampere per tip with high efficiency through the apertures.

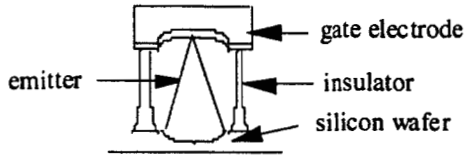

Fig. 6: Schematic of a Single Element of a Field Emitter Array

These cathodes are being developed commercially for use in vacuum devices such as flat panel displays, coherent radiation sources, ultra-fast logic circuits, and high power micro-wave amplifiers. Their small size, the fact that they can be batch-fabricated, and their ability to operate at very low power levels with no propellant make them attractive as electron sources for micro- or conventional-sized electric propulsion devices.

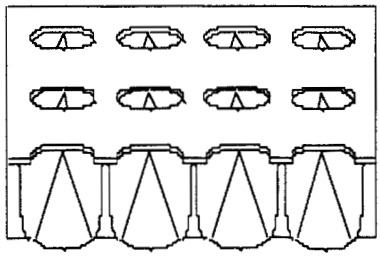

Fig. 7: Schematic of a Field Emitter Array

Field emitter array cathodes have not been used in the past with gas discharges because there was no way to protect the fragile tips from ion bombardment. The CLAIR electrode configuration is an innovative solution to the problem which opens up a variety of new applications. The CLAIR employs an electrostatic lens that filters out ions, focuses the electron beam and provides control over the energy of the emitted electrons. These functions are achieved by adding three electrodes with the appropriate thickness, inter-electrode spacing and voltages to the conventional FEAC geometry, as shown in Fig. 8.

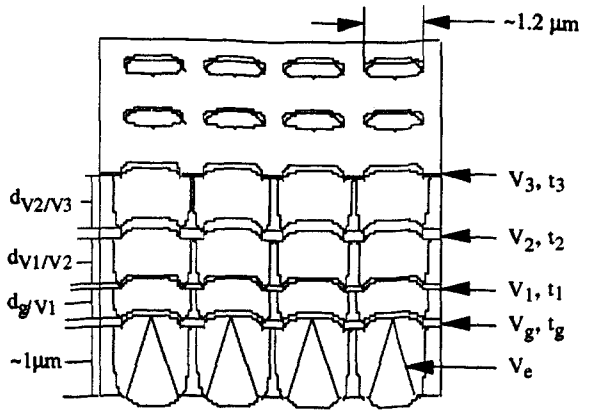

Fig. 8: FEAC Cathode Configuration with CLAIR.

The CLAIR structure includes electrodes V1, V2, and V3, which filter the ions, accelerate or decelerate the electron beam, and focus the electron beam. Ions entering the cathode will be retarded by the electric field between V2 and V3. V1, V2, and V3 create an electric field which focuses the electron beam through the high voltage grid V2. V3 also serves to shield the ion retarding grid from electrons in the ambient plasma. The voltage drop between Ve and V3 creates an electric field that accelerates or decelerates the electrons to the appropriate energy levels for the desired application.

Currently, while fabrication of stacked grid structures has begun to form the CLAIR grid configuration, testing of field emitter arrays fabricated from various materials is also being conducted. The goal of this activity is to seek out the most robust field emitter array cathodes, able to survive the longest in plasma environment at pressure greater than 10^{-5} Torr (Pressures inside a micro-ion engine will likely be much higher than 10^{-5} Torr, however, these tests also address needs for FEAs to be used as neutralizers for electric propulsion devices such as ion engines or Hall thrusters. In the thruster plumes of these devices, pressure will be lower than inside an ion engine, yet still significantly higher than in previous, commercial FEA applications, such as flat panel displays). Materials tested included silicon, molybdenum and hafnium-carbide forming the emitter tips. Test are ongoing.

Micro-Grids

Although the targeted micro-ion engine diameters of 1 -3 cm are such may not require microfabrication techniques to machine the engine body, a case can be made to investigate the feasibility of micromachined grid designs. Smaller diameter engines allow grids to be spaced much more closely with respect to each other since the amount of electrostatic-stress induced grid deformation will be less. Placing grids closer with respect to each other will increase the grid perveance, proportional to $1/d^2$, with d being the grid spacing. Thus, higher beam currents could be extracted form the engine for a given voltage, extending its performance range provided that sufficiently large ionization fractions can be provided in the ion engine plasma. However, ion optical considerations generally require grid aperture diameters to be scaled down in size with the grid spacing in order to avoid ion impingement on grids causing potentially engine life threatening grid erosion. Smaller aperture diameters, and the requirement to place apertures of the various grids (screen, accelerator, and, potentially, decelerator) of a grid system concentrically with respect to each other, requires tight machining tolerances. Current, "macro-machined" grids are fabricated within 0.05 mm, or 50 μm tolerances, representing a limit in most cases for many conventional machining techniques, such as electric discharge machining (EDM) or laser drilling for example. Using microfabrication techniques, however, much smaller tolerances can easily be obtained. In

addition, the ability to produce entire batch-fabricated grid systems, not requiring any additional assembly and grid alignment procedures, weighs in favor of microfabrication approaches as well.

The feasibility of grids based on silicon-based MEMS (Microelectromechanical Systems) machining techniques was thus explored. While other microfabrication possibilities exist, silicon-based MEMS techniques were investigated first due to the considerable heritage and experience available with this technique, as well as its demonstrated ability to produce extremely small feature sizes within very tight tolerances of 1 μm or less. However, MEMS-fabrication of accelerator grids opens up a host of fabrication and operations-related issues. Foremost among them is the selection of appropriate grid materials, suiting both microfabrication as well as grid operation needs, in particular with respect to sputter erosion and voltage stand-off characteristics. The grid insulator material, for example, isolating the screen and accelerator voltages from each other, will have to be able to stand off voltages on the order of 1.3 kV or more over distances on the order of a few microns if current grid voltages and engine specific impulses are to be maintained, as is desirable.

Silicon dioxide was investigated for use as a grid insulator material. Silicon dioxide was chosen since it exhibits good electric insulating characteristics when compared to other materials used in silicon-based MEMS fabrication, and is already widely used in the microfabrication field. In order to study the suitability of silicon oxide for this application, both bulk electric breakdown characteristics as well as electric breakdown characteristics along its surface needed to be studied. This is evident when inspecting Fig. 9. As can be seen, both modes of electric breakdown, substrate (or bulk) and surface, are possible in a typical grid design. The latter may occur along the walls of grid apertures. Two sets of experiments were conducted using specially designed silicon oxide breakdown test chips to systematically study both modes of electric breakdown, and will be described below.

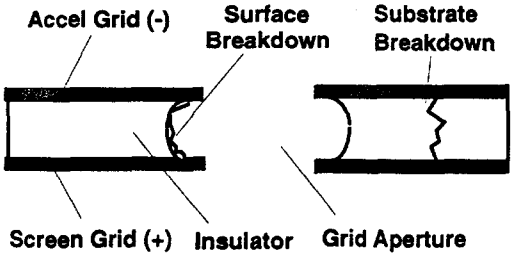

Fig. 9: Anticipated Grid Breakdown Modes

The here performed measurements can only be regarded as a first step in evaluating MEMS-based grid designs. Besides the always existing possibility that other insulators, deposited in modified and previously untried processes, may result in different breakdown characteristics, a key feasibility issue with respect to grid designs such as the one shown in Fig. 9 is the possibility of coating the insulator material along the exposed grid aperture wall surfaces with conducting, sputter-deposited material. Shadow-shielding around grid spacers is commonly used in grid system today, and similar concepts will need to be explored for microfabricated grids, and to be integrated into the batch fabrication process. Another important feasibility issue is sputter erosion of the various MEMS-grid materials considered. However, insulator grid breakdown was regarded as a logical starting point for a MEMS grid feasibility investigation to be followed up, if successful, in later studies by topics of considerably higher degrees of complexity in fabrication, such as insulator shielding.

The experiments (substrate, or bulk, and surface breakdown) were conducted with two types of test chips. A total of about 200 chips has been tested, of these 100 chips were used for substrate breakdown tests and 100 chips for surface breakdown tests. The chip type used for substrate breakdown is shown in Fig. 10. A detailed description of this chip was already given in

Ref. 43. Briefly, the chip consists of a silicon substrate, a doped polysilicon layer (serving as one of the two electrodes between which voltage is applied), a Low Temperature Oxide (LTO) layer and an aluminum contact pad, serving as the second electrode. Breakdown occurs through the oxide between the polysilicon layer and the aluminum pad. Each chip is 1 x 1 cm^2 in size. Polysilicon and oxide deposition were performed at the University of Berkeley. For some chips these fabrication steps were performed at the University of California/Los Angeles (UCLA). Samples of this latter batch of chips were also used in previous tests reported in Ref. 47. Depending on the desired oxide thickness, the oxide layer is etched back prior to aluminum evaporation. A via is etched into the oxide to provide access to the underlying polysilicon layer. An aluminum heater coil is also deposited onto the chip during the aluminum pad fabrication step. This (square-shaped) heater coil can be seen in Fig. 12 and is used to heat the chip for breakdown testing at elevated temperatures. Temperatures up to 400 C have been achieved with this design at power levels of about 11 W (160 V, 0.07 mA). Small variations in heater coil performance were found from chip to chip.

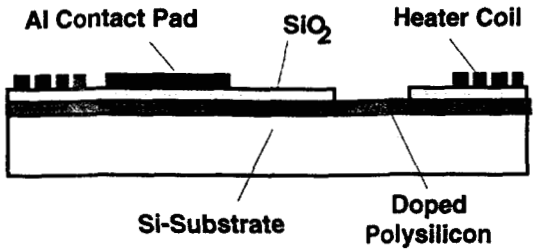

Fig. 10: Schematic of Substrate Breakdown Chip

Fig. 11: View of Substrate Breakdown Test-Chip

The substrate breakdown tests were performed under atmospheric conditions by placing the test chips into a specially designed quartz fixture, which in turn was placed underneath an infrared (IR) camera. The IR camera was used for temperature measurements but was also able to record arcing on the chip at ambient temperature. The chip was contacted via a probe station featuring four adjustable probe tips. Two tips served as high-voltage leads while the remaining two were used to contact the heater coil. Unfortunately the range of the probe tips was not large enough to test entire wafers. Therefore, wafers had to be diced into individual chips and the chips were tested one by one.

The design of the surface breakdown test chip varied slightly from substrate breakdown chip design. The surface breakdown chip design is shown schematically in Fig. 13. Again, a detailed description of this chip is given in ref. 43. The chip is of the same size as the substrate breakdown chip and very similar in appearance to the chip in Fig. 12, however, features smaller contact pad areas. In the case of the surface breakdown test chip, no doped polysilicon layer was deposited onto the silicon substrate. Instead LTO was deposited directly onto the substrate wafer.

Following was an aluminum deposition and pattern and etching of the aluminum to form the contact pads and heater coil. Aluminum pads were placed between 100 μm and 600 μm apart, in 100 μm increments. Later in the course of the experiment it was found that testing of molybdenum contact pads was considered desirable, and accordingly chips featuring contact pads made from this material were fabricated. Pads on that set of chips were separated by 5, 10, 20, 100, 200, and 300 μm, respectively, taking into account new data found with the previously described aluminum chips, indicating much higher surface breakdown strengths than measured in earlier tests. The surface breakdown chips were mounted into a different probe station, also featuring four probe tips, that could be attached to a Scanning Electron Microscope (SEM) vacuum stage. Pressures as low as 1 x 10^{-6} Torr could be obtained, although the majority of tests was performed at around 3 x 10^{-5} Torr, measured using the SEM stage pressure gage. This pressure level could be reached rather quickly using the existing pumping facilities. The vacuum stage of the SEM was turbomolecular pumped.

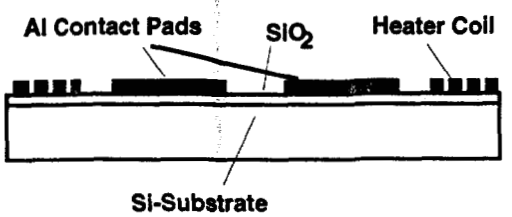

Fig. 13: Schematic of Surface Breakdown Chip

All chips were cleaned after dicing inside the microfabrication cleanroom facilities in an acetone ultrasonic bath for 10 minutes to remove contaminants and remaining photoresist traces, followed by an isopropyl alcohol rinse to remove remaining acetone residues, followed in turn by a dry, and were finally subjected to an oxygen plasma etch at 200 W for 10 minutes to remove remaining organic residue. The chips were then sealed inside plastic trays. The chips were left sealed inside those trays until the moment of usage, at which time they were subjected to the laboratory environment either for the duration of the test (substrate breakdown), or, in the case of the surface breakdown tests, for the duration it took to install one chip onto the probe station and pump down the system, typically a few minutes.

Substrate breakdown results are shown in Fig. 14 and 15. Measured data for LTO oxides were compared to data found in the literature for thermally grown oxides[48,49], RF sputtered oxides[50], as well as vapor deposited oxides on a glass substrate[51], using an evaporation process for silicon monoxide in an oxygen atmosphere. As can be seen, breakdown field strengths for LTO oxides range between 600 - 700 V/μm. Tests performed at elevated temperatures described in Ref. 43 revealed only a limited drop in breakdown field strength of about 15% as the temperature was increased from ambient to 400 C. These values compare well with RF and the vapor-deposited oxides by Klein and Gafni[51], however, are considerable less than breakdown field strengths found for thermally grown oxides. Note, however, that the high breakdown field strength values for thermally grown oxide were found for very small oxide thicknesses, and furthermore that thermally grown oxides can typically not be grown in excess of 2 micron. Thus, as Fig. 15 shows, voltage stand-off capability for thermally-grown oxide films is limited and much higher voltage stand-off capability can be obtained with LTO oxides. In the case of these experiments, voltages as high as 2500 V for a 3.9 μm film could be maintained. Thus, as far a bulk breakdown field strength is concerned, LTO oxide films appear suitable for use in ion engine grids. A somewhat different picture, however, emerges with respect to surface breakdown.

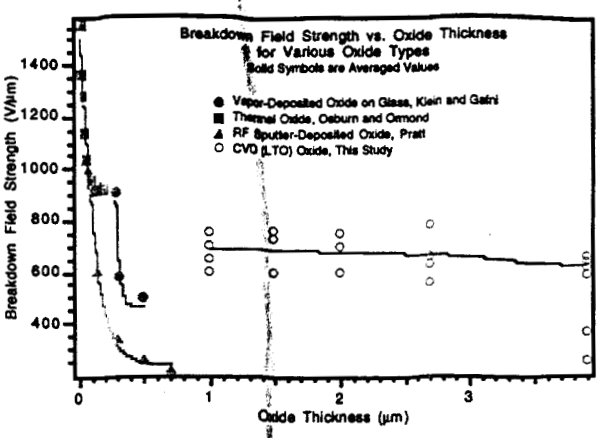

Fig. 14: Breakdown Field Strengths for Various Oxides vs. Oxide Thickness

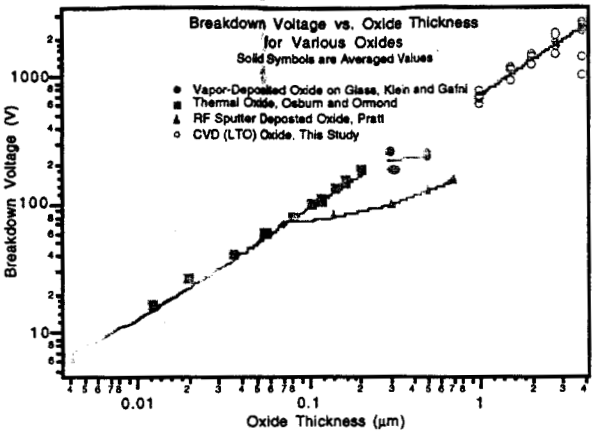

Fig. 15: Breakdown Voltages vs. Oxide Thickness for Various Oxides

As Fig. 16 shows, surface breakdown field strengths as high as 200 V/μm were measured over a gap distance between contact pads of 5 μm. Thus, if a 5 μm film thickness could be obtained, breakdown voltages that could be stood off along the grid aperture walls may be as low as 1 kV. Experiments, described in Ref. 43, were performed that excluded the possibility of Paschen breakdowns. Both aluminum and molybdenum contact pads were tested to exclude the possibility of material dependency of breakdown field strengths for these materials. It had been argued that hillocks forming on the aluminum surfaces might decrease breakdown field strengths. However, no such dependency was observed, in agreement with results reported by other researchers[49]. It therefore appears that surface breakdown field strengths of LTO oxides are not sufficient for these oxides to be used in ion engine grids. This experiment, however, does not precisely simulate the same geometry as found in microfabricated grids along aperture walls and thus any conclusions drawn have to remain preliminary.

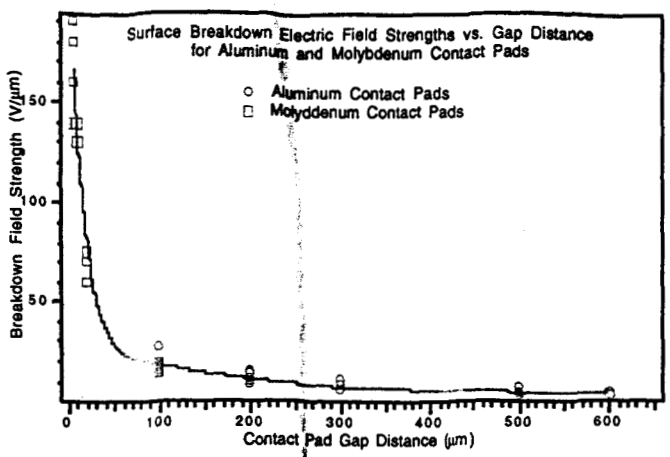

Fig. 16: Surface Breakdown Electric Field Strengths for LTO Oxide using Aluminum and Molybdenum Contact Pads vs. Pad Gap Distance

Experiments have been performed with chips featuring oxide undercuts fabricated underneath the contact pad edge, as shown in Fig. 17. Using this geometry, the sharp contact pad edge is not directly in contact with the oxide and it was hoped that breakdown filed strengths could thus be increased. However, as Table 2 shows, no such increase was observed. It is believed that the oxide etch also attacks the molybdenum contact pads used in these experiments, roughening those surfaces and therefore offsetting any benefits the undercut might have effected.

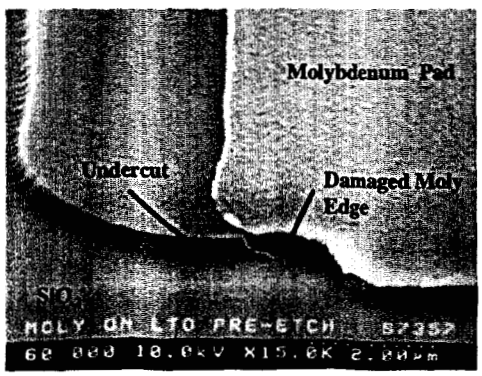

Fig. 17: Photo of Attempt to Achieve Oxide Undercut of Molybdenum Pad

Table 2: Surface Breakdown Voltages and Field Strengths for a 5 μm Gap using Oxide Undercut

Oxide Undercut (5 μm Gap)		**No Oxide Undercut (5 μm Gap)**	
Breakdown Voltage (V)	Breakdown Field Strength (V/μm)	Breakdown Voltage (V)	Breakdown Field Strength (V/μm)
600	120	700	140
600	120	700	140
900	180	700	140
900	180	800	160
1300	260	900	180
		900	180
		950	190

Future work will include the investigation of very thick Plasma Enhanced Chemical Vapor Deposited (PECVD) oxides at thicknesses up to 10 μm, provided by Alberta Microelectronic Corporation, non-silicon based micromachining methods, or the development of multiple grid structures. It may be possible to split the required voltage drop of about 1.3 kV between several grid pairs, the voltage drop between each pair being lower and inversely proportional to the total number of grids. Limits may arise as to how many grids may be stacked on top of each other due to intrinsic thin film stresses which may built up to the point that multiple thin films may begin to peel off their substrate. In this case, thermally grown oxides may become of interest again, as the required oxide thickness decreases in a multiple grid stack decreases and thermally grown oxides provide higher breakdown field strengths (at least as far as bulk breakdown is concerned, see Fig. 14).

V. MICRO-ISOLATION VALVE

As discussed above, at present several activities, in various stages of research and development, are underway in the propulsion field to address microspacecraft needs. Most of this work naturally focuses on thruster hardware. However, improvements in valve technologies with the goal to meet stringent mass, size, and power constraints expected to be found on a microspacecraft are also crucial to the success of micropropulsion concepts since it is important to ensure that the entire propulsion system weight and volume is reduced.

A normally closed isolation valve concept was introduced at JPL to address some of these needs. This valve concept is based in its fabrication on MEMS (Microelectromechanical Systems) technologies, resulting in a valve body approximately 1 x 1 x 0.1 cm^3 in size and weighing but a few grams, excluding fittings and packaging. This isolation valve, which can be opened only once, will serve to seal a propulsion system and provide zero leakage prior to actuation. Thus, the micro-isolation valve will serve the same function as a conventional pyro-valve. However, as will be seen below, no pyrotechnic actuation will be required in the micro-isolation valve concept. Propulsion system isolation is of particular importance for many interplanetary missions, where propulsion systems may not be activated until many years into the mission, following a long interplanetary cruise. During this time, propellant leakage will have to be avoided. For microspacecraft in particular, due to the limited onboard propellant supply, leakage rates will have to be minimized. Liquid propellants may be used in many applications, resulting in significantly reduced leak rates over gaseous propellants. However, in some cases the use of gaseous propellants may be unavoidable, such as for certain electric propulsion applications requiring xenon gas or for cold gas attitude control if spacecraft contamination concerns require the use of very benign propellants, such as nitrogen for example. Currently, no alternative to the relatively heavy and large scale pyrotechnically actuated valves exist typically used in these types of applications to seal the propulsion system. The micro-isolation valve is targeted to fill this gap.

While targeted for microspacecraft use, applications of the micro-isolation valve may also be found in more conventionally sized propulsion systems requiring only low flow rates, compatible with the to be expected small flow dimensions that could be provided on a chip. Such criteria may be fulfilled by certain electric propulsion systems, such as advanced ion and Hall thruster systems, requiring substantial dry weight reductions in its feed system designs.

The micro-isolation valve in its current form is a micromachined, silicon-based device that relies on the principle of melting a silicon plug, possibly doped to enhance its electrical conductance, which in the valve's normally closed position blocks the valve flow passage. Melting of the plug will open the valve and will be achieved by passing an electric current through the plug and resistively heating it. The valve will thus serve a similar function as a normally-closed pyrovalve, providing an essentially zero leak rate prior to actuation by completely sealing the flow passage. Unlike a pyrovalve, however, the here proposed valve will not rely on pyrotechnic actuation, thus avoiding the potential for pyroshocks as well as simplifying valve integration.

A schematic of the valve can be seen in Fig. 18. It consists of two basic components: the silicon chip featuring all the flow passages and valve inlet and outlet, and a Pyrex cover to seal the flow passages while allowing a view of the internal design of the chip for experimental evaluation of the concept. Later versions may be entirely assembled from silicon. The silicon-Pyrex bond is achieved by means of anodic bonding.

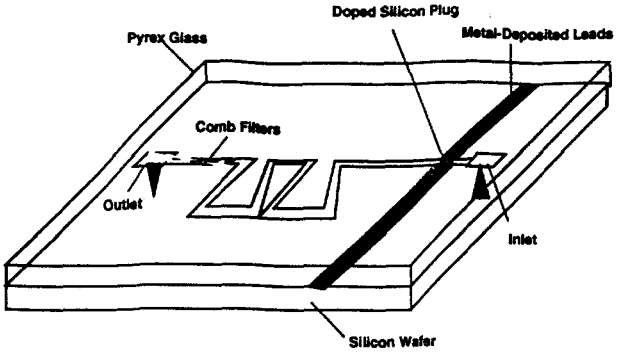

Fig. 18: Schematic of the Micro-Isolation Valve Concept

The silicon side of the chip features the valve-internal flow channels, the plug, and a filter, and will be batch-fabricated from larger silicon wafers. Channels in the chip are fabricated using deep trench reactive ion etching (RIE) techniques. This etching process is highly an-isotropic and allows deep features to be etched into the chip with very straight wall sections up to aspect ratios as high as 30:1. Metal (gold) leads deposited onto the silicon substrate, partially overlapping the doped-silicon plug region, will connect the plug to an external valve-opening circuitry. Propellant entering the valve chip will flow through a short channel section etched into the silicon side of the chip until it reaches the plug. Passing an electrical current through the plug will melt and/or vaporize it and propellant located upstream of the valve inlet will push the plug debris downstream, thus opening the valve. Figure 19 shows a close-up view of the plug region of a fabricated chip as viewed under an electron microscope.

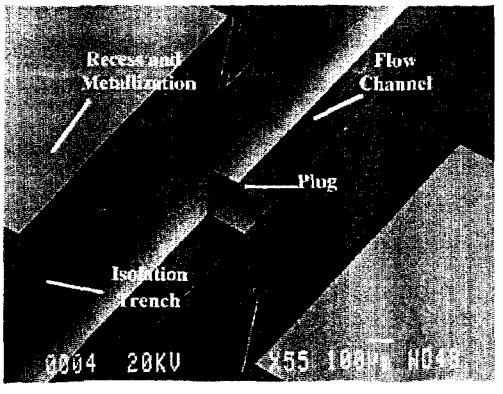

Fig. 19: Close-Up of Plug Area

Beyond the plug location the flow path continues. In order to prevent plug debris from contaminating flow components located downstream of the isolation valve, potentially clogging propellant lines, contaminating valve seats or otherwise interfering with the proper function of those components, it is crucial to trap the debris within designated, non-critical regions of the valve

without re-closing the flow path again. It is being speculated that due to melting rather than cold fracture of the plug debris count may be reduced and fewer, larger debris particles may be produced, which will be easier to trap. Nonetheless, filtration and other debris trapping schemes will be required.

Figure 18 shows one potential flow path configuration designed to accomplish this task. Here, the flow path goes through a series of S-shaped turns designed to trap molten plug debris in the corners of the etched channel. Oversizing the channel, in particular near the corners, will avoid clogging. Other configurations may be explored as the experimental program progresses, such as parallel flow passages for redundancy, for example. A comb filter integrated in the flow path downstream of the S-shaped condensation region will serve to trap debris that may not have been condensed at the flow path walls, but instead have solidified in the propellant stream. The comb filter uses a staggered filtration scheme , consisting of several rows of silicon posts. The spacing between the posts decreases for rows located further downstream, allowing larger particles to be trapped by upstream rows with wider post spacings and smaller particles by rows with narrower post spacings located further downstream, thus avoiding clogging of the filter. Using MEMS-based techniques, it is expected that very small filter ratings may be produced, into the μm-range.

Key feasibility issues to be addressed in the development of the isolation valve are melting of the silicon plug within acceptable power/energy levels, demonstration of sufficient pressure handling capability of the valve, in particular in view of high-pressure gas applications and in view of the thin plug barrier, and the aforementioned contamination and filtration concerns. At present, plug melting and pressure handling abilities of the valve have been addressed. These two issues are strongly related. Thermal considerations will drive the plug design to smaller thicknesses since a less massive plug is easier to melt, while pressure handling considerations will drive the plug design to larger thicknesses. A suitable trade-off between both extremes will need to be negotiated to arrive at a design addressing both concerns in a satisfactory manner.

Thermal Modeling of the Plug

In order to determine an appropriate valve plug design, the plug region of the valve was modeled thermally using a finite element package. The Finite Element Analysis (FEA) software used was PATRAN 6.0. In order to conserve computation time, only a quarter section of the plug, cut along two lines of symmetry, was modeled. In line with test chip design and fabrication considerations, the plug dimensions were chosen as 300 x 300 μm^2 (height x width), and two plug thicknesses, 10 μm and 50 μm, were considered. The thinner plug barrier will represent a thermally favored design, since melting this barrier will be easier to accomplish, while the thicker barrier will be favored based on pressure handling considerations.

Heating of the plug will occur resistively by passing an electric current through it. Since silicon is a semiconductor, it may be required to dope it to increase its electric conductance. Fabrication constraints are such that doping can only be achieved up to certain depths into the silicon due to diffusion limitations. Even using ion implantation techniques with a combined thermal drive-in, doped thicknesses of more than 10 μm can typically not be achieved. In the fabrication of the micro-isolation valve, wafers that feature epitaxially grown doped silicon layers are therefore being considered. These layers may be grown up to thicknesses of about 40 μm. Currently we have access to wafers featuring a 25 μm thick doped silicon epi-layer. Thus, heat maybe generated up to a depth of 25 μm into the barrier, and an according assumption was made in the FEA calculations. All calculations were performed for a normalized 1W total heater input power. Since this model relies entirely on heat conduction, governed by a linear relationship between temperature and power, temperature values can easily be extrapolated to other power levels. Test cases with this model were run to confirm this approach.

Figure 20 shows the case of a 10 μm thick plug (barrier) wall. Represented in this Figure is, as discussed, only a quarter section of the plug area. This section was obtained by both cutting the channel length-wise, along its center line, and then, in a perpendicular direction to the previous cut, dicing the barrier along its center plane. The part of the section extending above the height of the barrier wall in Fig. 20, i.e. the upper third of the section, represents the Pyrex cover. The lower two-thirds of the section represent the silicon wafer. The flow channel can be seen extending behind the plug. Thus, as represented in Fig. 20, only half the width and half the thickness of the barrier and only half the width of the channel extending behind the barrier is shown. Propellant would thus either flow into or out of the plane of the paper, if the barrier was open, depending on flow direction.

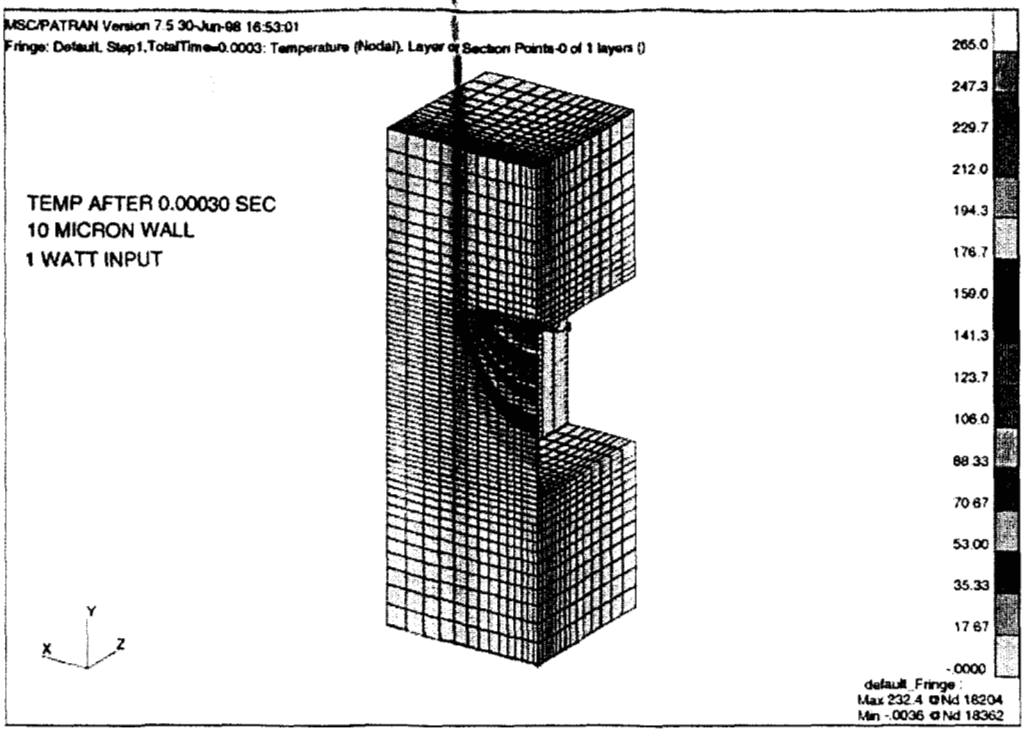

Fig. 20: Results of Thermal Modeling of Plug Quarter Section for a 10 μm Plug Thickness

As can be seen by inspecting Fig. 20, the peak temperature in this 1-W case reaches a value of 232 C in the center of the barrier near its top, where it bonds to the Pyrex, after only 0.3 ms. Thus, for a case of 10 W input power, which even without energy storage devices is not an unreasonable power level for a microspacecraft application, this temperature would be as high as 2320 C following a linear extrapolation as discussed above. Silicon melts at 1400 C. Thus, for a 10 W case, a substantial fraction of the barrier, approximately representing the upper 20% of the barrier, would reach melting temperatures, as can be seen by following the temperature contours in Fig.2. However, as the barrier starts to heat from the top where the electric current is flowing, the upper 25 μm, upon reaching melting temperature, may be removed, and the plug may thus loose the ability to conduct current and further heat addition may be prevented. Using the temperature plot and temperature contours in Fig. 20 results in a power estimate of about 7 W for a duration of 0.3 ms to melt the barrier to a depth of 25 μm measured from the top. These considerations do of course not take into account any influence the propellant pressure may exert onto the barrier. It is conceivable that due to softening of the silicon barrier prior to melting, and the application of

pressure onto barrier, even regions of the barrier which are below the actual melting point may break and be opened up.

Figure 21 shows the case of a plug of 50 μm thickness. Calculations were again performed for a normalized case of 1 W. After an on-time of 0.5 ms, comparable to the previously discussed 10-μm plug case, peak temperatures reached a value of about 58 C. Thus, in order to reach at least 1400 C in a comparable time period, approximately 1400/58 * 1 W = 24 W of power would be required over a duration of 0.5 ms. Given that the peak temperature shown in Fig. 3 is only reached at one location just below the top of the barrier, slightly higher power levels will likely be required in practice to heat the barrier to melting temperature to a depth of 25 μm. Using the plot in Fig. 21, for a melting temperature of 1400 C to a depth of 25 μm one may estimate a power requirement of about 28 W over a duration of 0.5 ms.

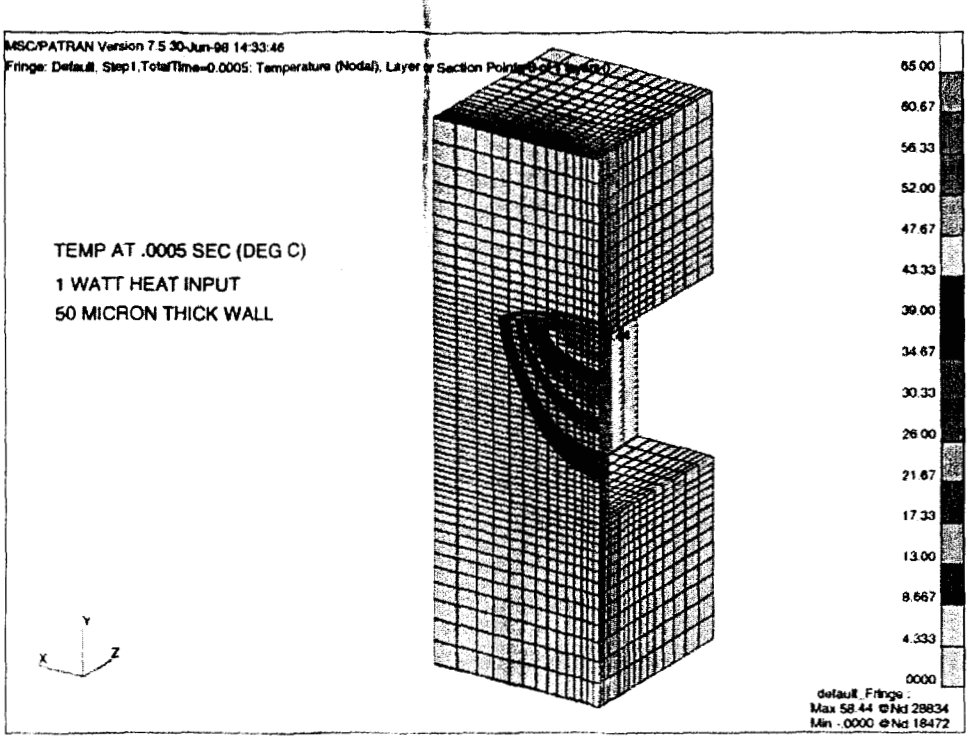

Fig.21: Results of Thermal Modeling of a Plug Quarter Section for a 50 μm Plug Thickness

While it may not be possible to remove the barrier in its entirety, an orifice located at the upper end of the barrier of about 25 μm in depth and of a comparable or larger width appears sufficient to allow for sufficient flow rates at very little pressure drops, even for liquid propellants, as was found out in related micropropulsion experiments recently conducted and discussed in a companion paper[4]. In that experiment, a vaporizing liquid micro-thruster chip featuring a 50 x 50 μm^2 inlet and a 50 x 50 μm^2 outlet, separated by a channel of similar dimensions and length as the one considered for the micro-isolation valve, showed no problems in passing appreciable amounts of fluids (water) at feed pressures of 10 psig and less. The flow channel dimensions in the micro-isolation valve will continue to be kept larger than the expected orifice in the barrier to reduce pressure drops inside the chip and to help avoid clogging of flow passages, in particular downstream of the plug region.

Thus the thermal analysis performed here seems to indicate that valve actuation is possible within power/energy constraints that may govern microspacecraft, although power values are

somewhat on the high side, in particular for the thicker plugs. For applications in larger systems, such as future electric propulsion feed systems where ample power should be available this may not be a concern. The aforementioned numerical results obviously need to be verified by experiments. Such experiments are scheduled immediately after completion of burst pressure tests to be discussed next.

Burst Pressure Tests

A set of test chips was fabricated to perform valve burst tests. Since the plug region was of particular interest in these tests, chips were fabricated that only featured the plug region, eliminating the downstream flow path and filter as seen in Fig. 18. An example of these chips can be seen in Fig. 23 and a schematic of this chip is shown in Fig. 24.

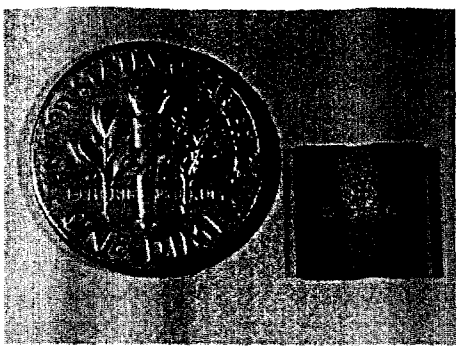

Fig. 23: Micro-Isolation Valve Test Chip

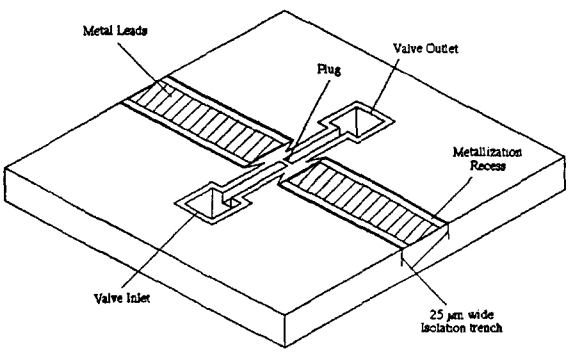

Fig. 24: Sketch of "Batch-2" Type Test Chip

Chips with different plug thicknesses were tested, including chips with plug thicknesses of 10, 15, 20, 25, 35 and 50 µm. Burst pressure data are plotted in Fig. 25. Two failure modes were observed. Chips with plug thicknesses of 20 µm or less failed due to plug breakage. An example of such a failure mode is shown in Fig. 26, showing a failed 20 µm plug which failed at 2,575 psig. Chips featuring plug thicknesses larger than 20 µm failed due to Pyrex breakage just above the chip inlet hole, as can be seen in Fig. 27. Burst pressure values are overall very impressive, considering that the valve consist of silicon and Pyrex only. The highest value recorded for a chip featuring a 50 µm plug (Pyrex failure) was 2,900 psig. Given that the failure was due to Pyrex breakage, it is conceivable that much higher burst pressure values may be obtained using thicker

Pyrex or another cover material, such as silicon. The Pyrex thickness at present is 0.5 mm. Current anodic bonding equipment limits the choice of Pyrex thicknesses to values less than 1.5 - 2 mm. The use of silicon cover material would require a re-design of the chip, eliminating the gold contacts since gold would melt during the subsequent high-temperature annealing steps required during silicon fusion bonding. However, if cover material breakage as shown in Fig. 27 can be avoided, Fig. 25 seems to indicate that burst pressure values would again follow the solid (Plug breakdown mode) curve which points to significantly higher burst pressure values for plug thicknesses of 20 μm and greater. Future valves maybe tailored for their respective application. A liquid propellant application, for example, typically featuring much lower feed pressures on the order of 300 psia or so, may only require a 15 - 20 μm thick plug which would reduce power requirements to melt the plug. Cold gas applications will require larger plug thicknesses depending on storage pressure. Ten micron thick plugs appear not very useful for either application.

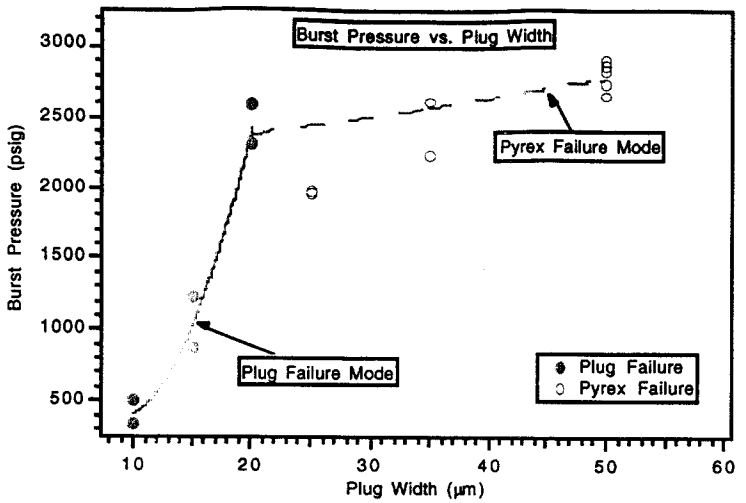

Fig. 25: Burst Pressure vs. Plug Width

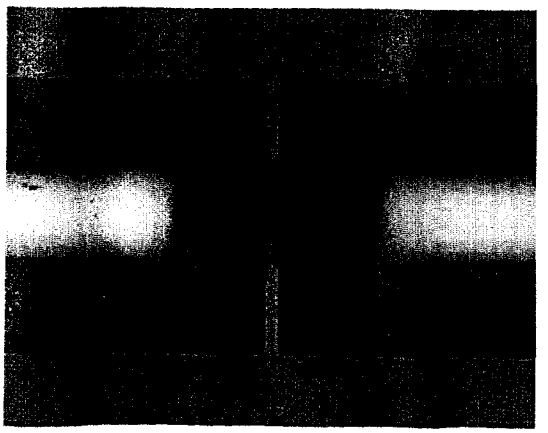

Fig. 26: Plug (Barrier) Failure (20 μm plug width, Burst @ 2575 psig)

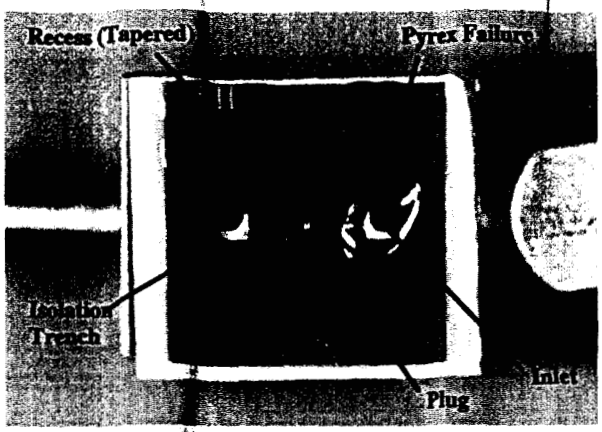

Fig. 27: Post-Test Image of Burst "Batch-2" Type Chip. Notice Hole in Pyrex over Inlet.

VI. OTHER ACTIVITIES

In addition to the MEMS propulsion activities described in greater detail in this paper, other micropropulsion activities are also being pursued at JPL today. A MEMS-based piezoelectric valve is being developed at JPL's Micro Devices Laboratory (MDL). Several SBIR programs focusing on micropropulsion devices have been monitored through JPL, such as two programs (Phase II) conducted by Marotta Scientific Controls, developing MEMS-hybrid cold gas thruster concepts and a MEMS-based flow controller, termed a Micro-Gas Rheostat. Another contract (Phase I) is dedicated to develop a MEMS-based flow meter to measure very small gas flows. Propulsion system designs are also being explored in support of future X-2000 missions as well as other microspacecraft activities, explored under JPL's Micro/Nano Spacecraft Technology Program (MNTD).

VII. CONCLUSIONS

Future microspacecraft designs, featuring spacecraft wet masses of a few tens of kilograms or less, will require the development of radically new subsystem and component designs. Progress is currently being made in several areas, such as instrumentation or attitude control sensing. Propulsion will likely be a key component on future microspacecraft, providing attitude control and the ability to change trajectories to meet mission needs. However, developments in micropropulsion, in particular addressing smaller microspacecraft designs in the sub-10 kg mass range, appear still severely lacking. Recently, advances in the development of MEMS propulsion concepts have been made to address these needs. Work on such concepts is in its earliest stages, underscoring the advanced nature of these propulsion technologies, and is being performed at a variety of institutions in the US and abroad. Several advanced micropropulsion activities under study at JPL were discussed in greater detail, including a so called Vaporizing Liquid Micro-Thruster (VLM), Micro-Ion Engine technologies and a Micro-Isolation Valve (MIV).

Proof-of-concept tests have recently been performed for a VLM thruster, resulting in complete propellant (water) vaporization at 2 W and 2 V. Within the micro-ion engine thrust, filed emitter array cathodes are being studied with the goal of adapting present technologies to the punishing plasma environment that may be found in electric thruster plumes and engine plasmas, possibly leading to erosion and lifetime concerns for this technology. To address these issues, different field emitter materials as well as batch-fabricated, integrated grid structures are being studied, aimed at repelling plasma ions which could erode field emitter tips.

Micro-isolation valves were shown to be able to withstand internal pressures of up to 2,900 psig before bursting. For valve chips featuring thicker plugs (> 20 μm) the failure mode was determined to be bursting of the Pyrex cover glass. Using thicker Pyrex material or silicon as a

cover material is believed to increase burst pressures even further. Numerical finite element calculations have shown that plug vaporization may be possibly with 30 W over a time interval of 0.5 ms to melt a 50 μm plug. The required power values drop significantly for thinner plugs. For example, a 10 μm plug may be molten at power levels of 10 W over roughly 0.5 ms. Further optimization of plug design will be required to result in plug widths with optimized thicknesses, able to withstand the desired operating pressure of the valve while minimizing power requirements to actuate the valve.

VIII. ACKNOWLEDGMENTS

The research described in this paper was carried out by the Jet Propulsion Laboratory, California Institute of Technology, under a contract with the National Aeronautics and Space Administration. The work was funded by the JPL Director's Research Discretionary Fund and support is gratefully acknowledged.

IX. REFERENCES

[1]Mueller, J., "Thruster Options for Microspacecraft: A Review and Evaluation of Existing Hardware and Emerging Technologies", AIAA Paper 97-3058, 33rd Joint Propulsion Conference, July 6-9, 1997, Seattle, WA.

[2]Collins, D., Kukkonen, C., and Venneri, S., "Miniature, Low-Cost Highly Autonomous Spacecraft - A Focus for the New Millennium", IAF Paper 95-U.2.06, Oslo, Norway, Oct. 1995.

[3]Blandino, J., Cassady, R., and Sankovic, J., "Propulsion Requirements and Options for the New Millennium Interferometer (DS-3) Mission", AIAA 98-3331, 34th Joint Propulsion Conference, Cleveland, OH, July 13 - 15, 1998.

[4]Strand, L., Toews, H., Schwartz, K., and Milewski, R., "Extended Duty Cycle Testing of Spacecraft Propulsion Miniaturized Components", AIAA Paper 95-2810, San Diego, CA, July 1995.

[5]Mueller, J., Vargo, S., Chakraborty, I., Forgrave, J., Bame, D., and Tang, W., "The Micro-Isolation Valve: Introduction of Concept and Preliminary Results", AIAA Paper 98-3811, 34th Joint Propulsion Conference, July 13-15, 1998, Cleveland, OH.

[6]Mitterauer, J., "Prospects of Liquid Metal Ion Thrusters for Electric Propulsion", IEPC Paper 91-105, Viareggio, Italy, Oct. 1991.

[7]Janson, S., "Chemial and Electric Micropropulsion Concepts for Nanosatellites", AIAA Paper 94-2998, 30th Joint Propulsion Conference, June 27-29, 1994, Indianapolis, IN.

[8]Jones, R., "JPL Microspacecraft Technology Development (MTD) Program", JPL Internal Document, May 31, 1996.

[9]Jones, R.,"Electromagnetically Launched Micro-Miniature Spacecraft for Space Science", JPL New Technology Report NPO-17338/6846, 6/18/87.

[10]Jones, R. M., "Electromagnetically Launched Micro Spacecraft for Space Science Mission", Journal of Spacecraft and Rockets, vol. 26, # 5, Sept - Oct, 1989, p. 338

[11]Jones, R. M., "Coffee-Can Sized Spacecraft", Aerospace America, October1988.

[12]Jones, R. M.,"Microspacecraft Missions and Systems", Journal of the British Interplanetary Society, Vol. 42, # 10, October 1989.

[13]Jones, R. M., "Think Small but in Large Numbers", Aerospace America, October 1989.

[14]Jones, R.M. and Salvo, C.G., "Microspacecraft Technology for Planetary Science Missions", IAF-91-51, 42nd Congress of the International Astronautical Federation, Montreal Canada, October 5-11, 1991.

[15]Burke, J.D.,"Micro-Spacecraft ", JPL Publication 715-87, 10/15/81.

[16]Staehle, R. L.,"Small Planetary Missions for the Space Shuttle", AAS Paper 79-288, 10/29/79.

[17]Mueller, J., "Propulsion Options for Microspacecraft", JPL Internal Document, JPL-D-13444, Dec. 4, 1995.

[18]West, J., "Microelectromechanical Systems (MEMS)/Nanotechnology Studies", JPL Internal Document, JPL-D-13302, January 12, 1996.

[19]Mueller, J., Chakraborty, I., Bame, D., Tang, W., and Wallace, A., "Proof-of-Concept Demonstration of a Vaporizing Liquid Micro-Thruster", AIAA Paper 98-3924, 34th Joint Propulsion Conference, Cleveland, OH, July 13-15, 1998.

[20]Stenmark, L. and Lang, M., "Micro Propulsion Thrusters and Technologies", Proc. Second European Spacecraft Propulsion Conference, ESA SP-398, pp. 399-405. May 27-29, 1997, ESTEC, Noordwijk, The Netherlands.

[21]Stenmark, L., Lang, M., Köhler, J., and Simu, U., "Micro machined Propulsion Components", Proceedings, 2nd Round Table on Micro/Nano Technologies for Space, ESA WPP-132, pp. 69-76, Oct. 15-17, 1997, ESTEC, Noordwijk, The Netherlands.

[22]Stenmark, L., "Micro Machined Cold Gas Thrusters", Proceedings, Workshop on Low Cost Spacecraft Propulsion Technologies for Small Satellites, March 19-20, 1998, ESA-ESTEC, Noordwijk, The Netherlands.

[23] Dilhan, D., "Small Rocket Motors for Micro Satellites", Proceedings, ESA Workshop on Low Cost Spacecraft Propulsion Technologies for Small Satellites, March 19-20, 1998, ESTEC, Noordwijk, The Netherlands.

[24]Lewis, D., Antonsson, E., and Janson, S., "MEMS Microthruster Digital Propulsion System", Proceedings, Formation Flying and Micro-Propulsion Workshop, Air Force Research Laboratory (AFRL), Oct. 20-21, 1998, Lancaster, CA.

[25]Youngner, D. and Choueiri, E., "MEMS Mega-Pixel Microthruster Arrays for Micro-Satellites", Proceedings, Formation Flying and Micro-Propulsion Workshop, Air Force Research Laboratory (AFRL), Oct. 20-21, 1998, Lancaster, CA.

[26]Perel, J., Mahoney, J., and Sujo, C., "Micro-Electric Propulsion Using Charged Clusters", Proceedings, Formation Flying and Micro-Propulsion Workshop, Air Force Research Laboratory (AFRL), October 20 - 21, 1998, Lancaster, CA.

[27]Pearson, E. and Schwoebel, P., "Microfabricated Field Ionization Thrusters", Proceedings, Formation Flying and Micro-Propulsion Workshop, Air Force Research Laboratory (AFRL), Oct. 20-21, 1998, Lancaster, CA.

[28]Marcuccio, M., Lorenzi, G., and Andrenucci, M., "Development of Miniaturized Field Emission Electric Propulsion System", AIAA Paper 98-3919, 34th Joint Propulsion Conference, July 13-15, 1998, Cleveland, OH.

[29]Yashko, G., Giffin, G., and Hastings, D., "Design Considerations for Ion Microthrusters", IEPC Paper 97-072, 25th International Electric Propulsion Conference, August 24-28, 1997, Cleveland, OH.

[30]Bayt, R., Ayon, A., and Breuer, K., "A Performance Evaluation of MEMS-based Micronozzles", AIAA paper 97-3169, 33rd Joint Propulsion Conference, July 7-9, 1997, Seattle, WA.

[31]Breuer, K. and Bayt, R., "Viscous Effects in Supersonic MEMS-Fabricated Micronozzles", Proceedings, Formation Flying and Micro-Propulsion Workshop, Air Force Research Laboratory (AFRL), Oct. 20-21, 1998, Lancaster, CA.

[32]Reed, B., "Micropropulsion Activities at NASA Lewis Research Center", Proceedings, Formation Flying and Micro-Propulsion Workshop, Lancaster, CA, Oct. 20-21, 1998.

[33]Martinez-Sanchez, M., "Advances in Micro-Propulsion: 50W Hall Thruster, Colloidal Thrusters", Proceedings, Formation Flying and Micro-Propulsion Workshop, Oct. 20-21, 1998, Lancaster, CA.

[34]Khayms, V. and Martinez-Sanchez, M., "Design of a Miniaturized Hall Thruster for Microsatellites", AIAA Paper 96-3291, Lake Buena Vista, FL, July 1996.

[35]Khayms, V. and Martinez-Sanchez, M., "Preliminary Experimental Evaluation of a Miniaturized Hall Thruster", IEPC Paper 97-077, 25th International Electric Propulsion Conference, August 24-28, 1997, Cleveland, OH.

[36]Young, M., Muntz, E., and Ketsdever, A., "Investigation of a Candidate Non-Magnetic Ion Micro-Thruster for Small Spacecraft Applications", AIAA Paper 98-3917, 34th Joint Propulsion Conference, Cleveland, OH, July 13-15, 1998.

[37]Spanjers, G., "Micro-Propulsion Research at the Air Force Research Laboratory", Proceedings, Air Force Research Laboratory Formation Flying and Micro-Propulsion Workshop, Oct. 20-21, 1998, Lancaster, CA.

[38]Ketsdever, A., Wadsworth, D., Vargo, S., and Muntz, E., "The Free Molecule Micro-Resistojet: An Interesting Alternative to Nozzle Expansion", AIAA Paper 98-3918, 34th Joint Propulsion Conference, July 13-15, 1998, Cleveland, OH.

[39]de Groot, W., Reed, B., and Brenizer, D., "Preliminary Results of Solid Gas Generator Micro-Propulsion", AIAA Paper 98-3225, 34th Joint Propulsion Conference, July 13-15, 1998, Cleveland, OH.

[40]Janson, S., "Batch-Fabricated Resistojets: Initial Results", IEPC Paper 97-070, 25th International Electric Propulsion Conference, Aug. 24-28, 1997, Cleveland, OH.

[41]Janson, S., "Chemial and Electric Micropropulsion Concepts for Nanosatellites", AIAA Paper 94-2998, 30th Joint Propulsion Conference, June 27-29, 1994, Indianapolis, IN.

[42]Janson, S. and Helvajian, H., "Batch-Fabricated Microthrusters: Initial Results", AIAA Paper 96-2988, 32nd Joint Propulsion Conference, July 1-3, 1996, Lake Buena Vista, FL.

[43]Mueller, J., Pyle, D., Chakraborty, I., Ruiz, R., Tang, W., and Lawton, R., "Microfabricated Ion Accelerator Grid Design Issues: Electric Breakdown Characteristics od Silicon Dioxide Insulator Material", AIAA Paper 98-3923, 34th Joint Propulsion Conference, July 13-15, 1998, Cleveland, OH.

[44]Marrese, C., Polk, J., Jensen, K., Gallimore, A., Spindt, C., Fink, R., Tolt, Z., and Palmer, W., "An Investigation into the Compatibility of Field Emission Cathode and Electric Thruster Technologies: Theoretical and Experimental Performance Evaluations", to be published, *J.Propulsion.*

[45]Marrese, C., Wang, J., Goodfellow, K., and Gallimore, A., "Modeling of Space-Charge Limited Emission from Filed Emission Array Cathodes for Electric Propulsion Systems and Tether Applications", to be published, *J.Propulsion.*

[46]Jahn, R.G., Physics of Electric Propulsion, McGraw-Hill, New York, 1968.

[47]Mueller, J., Tang, W., Li, W. , and Wallace, A., "Micro-Fabricated Accelerator Grid System Feasibility Assessment for Micro-Ion Engines", IEPC 97-071 Paper, 25th International Electric Propulsion Conference, Aug. 1997, Cleveland, OH.

[48]Osburn, C.M. and Ormond, D.W., "Dielectric Breakdown in Silicon Dioxide Films on Silicon, Part I", *J.Electrochem.Soc.*, Vol.119, No.5, pp.591-597, May 1972.

[49]Osburn, C.M. and Ormond, D.W., "Dielectric Breakdown in Silicon Dioxide Films on Silicon, Part II", *J.Electrochem.Soc.*, Vol.119, No.5, pp. 597-603, May 1972.

[50]Pratt, I.H., "Thin-Film Dielectric Properties of RF Sputtered Oxides", *Solid State Technology*, pp. 49-57, Dec. 1969.

[51]Klein, N. and Gafni, H., "The Maximum Dielectric Strength of Thin Silicon Oxide Films", *IEEE Transactions on Electron Devices*, Vol. ED-13, No.12, Feb. 1966.